**International Journal on Recent Researches in Science, Engineering & Technology (IJRRSET)**

**A Journal Established in early 2000 as National journal and upgraded to International journal in 2013 and is in existence for the last 10 years. It is run by Retired Professors from NIT, Trichy. Journal Indexed in JIR, DIIF and SJIF.**

**Available online at:** www.jrrset.com

**Received on:** 04.12.2019 **Published on:** 21.01.2020 **Pages :** 64-70

ISSN (Print) : 2347-6729
ISSN (Online) : 2348-3105

**Volume 7, Issue 12**
**December 2019.**
**JIR IF : 2.54**
**SJIF IF : 4.334**
**Cosmos: 5.395**

# Enhanced Photocatalytic Degradation of Textile Dye Using W, N Co-Doped ZnO Powder: Synthesis, Characterization, and Solar Activity

**Thamizhselvi D, Revathi A, Vasanthi M, Ramya K**
Department of Science and Humanities, A.R. Engineering College, Vadakuchipalayam, Villupuram-605601, Tamil Nadu. *Corresponding Author: E-Mail: thamizhkymari2020@gmail.com

**Abstract:** The photocatalytic degradation of Reactive Blue 4 (RB 4) under solar irradiation was investigated using W, N co-doped ZnO. Various mole ratios (0.02 mol%, 0.03 mol%, 0.04 mol%, 0.05 mol%, and 0.06 mol%) of W, N co-doped ZnO photocatalysts were prepared via the sol-gel technique. Pure ZnO exhibited low photocatalytic activity due to poor surface properties, photo-corrosion, and limited utilization of visible light. These drawbacks were mitigated by doping ZnO with W, N. The photocatalytic activity of W, N co-doped ZnO significantly surpassed that of pure ZnO. XRD, SEM, UV-DRS, PL, and FTIRB analyses confirmed the enhanced photocatalytic properties of W, N co-doped ZnO. Furthermore, W, N co-doped ZnO exhibited photostability and long-term durability.

**Keywords:** W, N Codoped ZnO, Sol-gel route, photocatalytic degradation, Reactive Blue 4, solar light

## 1. INTRODUCTION

The last centuries have seen a steady increase in human activities, causing remarkable technological development and soaring human populations. However, the industrial expansion has brought atmospheric, ground, and water pollution, all harmful to humans and the environment. Indeed, major pollution can cause human diseases like breathing problems, cardiovascular problems, cancers, neurobehavioral disorders, etc. It can also affect global warming, which worsens climate change, increases sea level rises, and causes serious damage to animals and flora.

Among the water pollutants, synthetic dyes pose significant issues. Synthetic dyes are commonly used by various industries, especially textile ones. These physically and chemically stable compounds are harmful to the environment. Synthetic dyes are recalcitrant compounds that exhibit high solubility in water and accumulate in both wastewater and industrial effluents. Consequently, the recovery of wastewater by conventional methods is not suitable for emergent pollutants. Heterogeneous photocatalysis can be satisfactorily applied for the decontamination of natural samples through the photocatalytic degradation of toxic pollutants from complex matrices, such as river water and wastewater. All renewable technologies have become a promising alternative for both energy generation and wastewater treatments. Solar photocatalysis is a suitable option to degrade recalcitrant pollutants from water.

The absorption of a photon initiates the photodecomposition of a semiconductor with energy greater than or equal to the bandgap of the semiconductor, producing electron-hole pairs. It is important for prolonging electron-hole recombination before a designated chemical reaction occurs on the semiconductor surface. Several semiconductor photocatalysts such as $TiO_2$, ZnO, $WO_3$, $SnO_2$, CdS, and ZnS have been used for the treatment of wastewater pollutants under visible light irradiation. Among semiconductors, zinc oxide (ZnO) has attracted attention due to its environmental stability as compared to other metal oxides. The application of photocatalysis, especially using semiconductors such as ZnO, appears to be a more appealing option.

**Approach to Photocatalysis**

ZnO serves as a superior alternative to conventional chemical oxidation methods for the decomposition of toxic compounds due to its nonhazardous product[12]. This is because semiconductors have unique properties such as inexpensive, non-toxic, high surface area, broad absorption spectra, and facilitating multi-electron transfer processes. ZnO has been demonstrated as an improved photocatalyst as compared to commercialized $TiO_2$ based on its more significant rate of activities and higher absorption efficacy of solar radiations[13]. However, ZnO has almost the same bandgap as $TiO_2$. Surface area and surface defects play an essential role in the photocatalytic activities of metal oxide. The photocatalytic activity of ZnO is restricted to the irradiation wavelengths in the UV region because of its wide bandgap of about 3.2 eV and low quantum efficiency[14]. The fast recombination of ZnO's electrons poses additional constraints to its application. Some alternative strategies to extend ZnO's photoresponse in the visible light region are: (a) ZnO doping[15], (b) co-doping [16], (c) coupling with lower band gap semiconductors[17], (d) surface plasmon resonance[18], (e) quantum dots[19], and (f) sensitization with natural and synthetic dyes[20].

Several attempts have also been made to improve the efficiency of photocatalysts by using doping materials. Doping is required to improve the efficiency of photocatalysts. The reduction of the optical energy gap of ZnO by doping is an advantage for use in photocatalytic devices. Among these doping materials, Ag-doped ZnO[21], N-doped ZnO[22], Mg-doping on ZnO[23] shows good photocatalytic activity.

Doping of non-metallic elements can form an intermediate energy level in the band gap of ZnO, which can reduce the band gap of ZnO and increase the photocatalytic activity of visible light. Anion doping can achieve better optical response of ZnO, especially in V group elements N, P, As[24]. Substitution by N doping is one of the best ways to lower down the band gap of ZnO, owing to the atomic size and electronegativity of the non-metal element N and the closest to O atom[25], and the mixing p state of N and 2p state of O narrow the band gap of semiconductor oxide[26]. Furthermore, the introduction of N atoms into ZnO lattice will bring the energy band into intermediate energy level and reduce the absorption energy, which can increase photocatalytic activity[27].

The combination between the properties of the nonmetals with that of transition metals may induce desirable optical and photocatalytic properties in ZnO. The integration between the visible-light responsive properties of nonmetal and the metal as trap centers can prompt more efficiency for practical applications. A. M. Youssef and S. M. Yakout designed effective visible light photocatalysts composed of C/La or Ce codoped ZnO nanostructures were prepared by sol gel method.

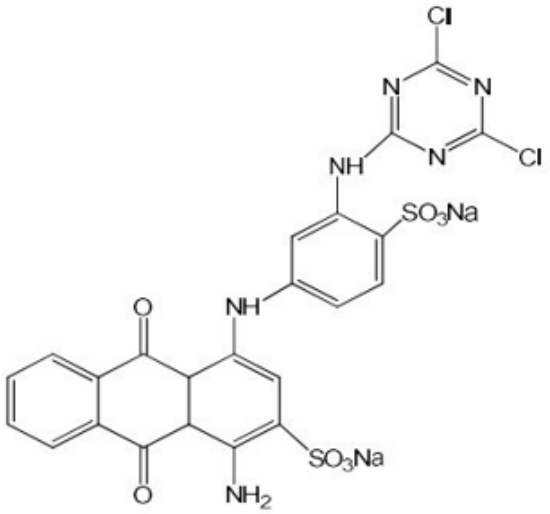


Chemical structure of Reactive Blue 4

**2.2. Preparation of W, N- codoped ZnO photocatalyst**

10 g of zinc chloride and 0.01 mol% of Sodium tungstate and Urea were dissolved in 100 ml of double distilled water for the preparation of W, N- codoped ZnO photocatalyst. The dopant concentrations were added at the ratios like 0 to 0.05 mol percentage. To that solution required amount of sodium bicarbonate was then added in portions with vigorous stirring for several minutes, finally the precipitate was formed. The doped photocatalysts are washed several times with distilled water to remove NaCl formed. The precipitate was then dried at 100°C to remove the water. The obtained precipitate was grinded in an agate mortar and pressed into a ceramic

crucible. The material was calcinated at 500°C for 4 hrs. The undoped ZnO was also synthesized in the same procedure without adding dopant concentration.

### 2.3. Characterization

X-ray powder diffraction (XRD) patterns of the photocatalysts were recorded on a Philips X'pert-MPD diffractometer in the 2θ range 20-80° using Cu-Kα radiation. The data were collected with a step of 0.028°. The atom temperature. Determe structure of the products was determined by comparing the experimental X-ray powder patterns to the standard compiled by the Joint Committee on Powder Diffraction and Standards (JCPDS). The crystallite sizes were calculated from the peak width using the Scherrer equation. The surface morphologies and particle size were observed by Scanning Electron Microscopy (JEOL, JSM-6360LV). UV-Visible diffuse reflectance spectra were acquired by a PerkinElmer Lambda 35 spectrometer. BaSO4 was used as the reflectance standard. The photoluminescence emission spectra of the samples were measured at room temperature using Perkin-Elmer LS 55 Luminescence spectrophotometer.

### 2.4. Photocatalytic studies

#### 2.4.1. Photocatalytic degradation study of RB 4

All the photocatalytic experiments were performed under natural sunlight on clear sky days during the period of June to October 2020. In a typical experiment, 50 ml of dye solution (concentration 50 mg·l^-1) was taken with 50 mg of photocatalyst in a 250 ml glass beaker. Then the dye solution was kept in direct sunlight with continuous aeration and the concentration of the dye remains was measured periodically by measuring its light absorbance at the visible λ_max by using Elco SL-171 Visible spectrophotometer. To avoid variation in results due to fluctuation in the intensity of the sunlight, a set of experiments have been carried out simultaneously. For pH studies the pH of the dye solutions were modified to different values (3, 5, 7, 9 and 12) by using 0.1M HCl and NaOH solution.

#### 2.4.2. Chemical Oxygen Demand Analysis

The chemical oxygen demand (COD) is the indirect measurement of the oxygen needed for the complete oxidation of all the compounds present in solution. The COD of the degraded dye solution were analyzed in standard dichromate method. For the analysis, 0.4g of HgSO4 was added to 20ml of the degraded dye solution in a 250 ml round bottom flask. To that 10ml of 0.25N $K_2Cr_2O_7$ was added and mixed well. Then 30 ml of $H_2SO_4$-$Ag_2SO_4$ reagent (prepared by dissolving 0.5g of $Ag_2SO_4$ in 30ml of Concentrated $H_2SO_4$) was added slowly with constant stirring. After that few pieces of pumice stones were added and the flask was fitted with a condenser and refluxed for 2 hours. The solution was cooled and diluted to 150ml with distilled water and the entire content was titrated against 0.25N Ferrous Ammonium Sulphate (FAS) solution using ferroin as indicator.

$$\text{COD in mg·l\^-1} = (V_1 - V_2) \times N \times 8 \times 1000 VsampVsamp1000$$

Where $V_1$ & $V_2$ are the volume of FAS solution consumed for blank and test sample respectively, N is the normality of FAS solution and $VsampVsamp$ is the volume of sample taken for analysis.

## 3. RESULTS AND DISCUSSION

### 3.1 Physicochemical characterization of the photocatalyst

#### 3.1.1 X-ray Diffraction Studies

The powder XRD patterns of ZnO and 0.04 mol% W, N- codoped ZnO were as shown in Figure 1. Both samples were identified as a single phase wurtzite ZnO by XRD analysis (JCPDS card nos.: 89-1397, 89-0511). The W, N codoped ZnO shows high intensity of the peaks, indicating that the samples are highly crystalline. On the other hand, codopants such as W and N incorporation on ZnO lattice increased the crystallinity. The mean crystallite sizes of the samples calculated by using the Scherrer formula for ZnO and W, N- codoped ZnO was given in Table 1. The results show that W, N doping decreases the particle size of the ZnO. An XRD pattern of W, N- codoped ZnO indicates the uniform dispersion of W and N ions. Moreover, the bulk structure remains virtually unchanged by the W and N- incorporation.

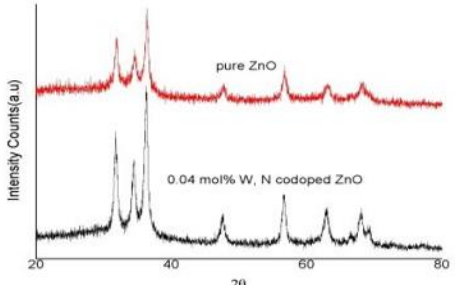


**Figure 1: XRD patterns of ZnO and W, N- codoped ZnO.**

**Table 1: XRD Calculation Results of ZnO and W, N- codoped ZnO**

| Photocatalyst | d(101)-spacing (Å) | Full Width Half Maximum (nm) | Average Crystallite Size (nm) |
|---|---|---|---|
| ZnO | 2.4753 | 0.342° | 73 |
| 0.04% W, N- codoped ZnO | 2.4710 | 0.400° | 38 |

### 3.1.2 SEM Analysis of the Photocatalyst

The SEM micrographs of ZnO and 0.04% W, N- codoped ZnO photocatalysts were shown in Figure 2 a, b respectively. The micrographs show that ZnO particles have blunter particle morphology whereas W, N-codoped ZnO has irregular arrangement patterns composed of spherical ZnO. This type of morphology could be able to completely degrade dye solutions. The reason is doped photocatalyst has shown a highly rough surface.

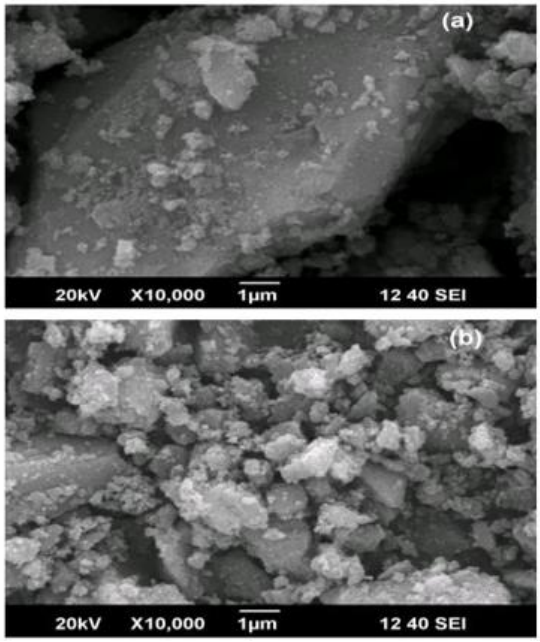


**Figure 2: SEM micrograph of (a) ZnO, (b) 0.04% W, N codoped ZnO photocatalyst.**

### 3.1.3 Diffused Reflectance UV-Visible Analysis of the Photocatalyst

Diffused reflectance spectra UV-visible spectra of ZnO and W, N- codoped ZnO absorption in Figure 3. The results show that the absorption onset of ZnO and W, N- codoped ZnO were 390 nm and 480 nm respectively. Therefore W, N- codoped ZnO can utilize visible light than the pure ZnO for photoexcitation process and expected to have more activity in the solar radiation than the undoped ZnO. The red shift in the light absorption of ZnO on W and N doping has been interpreted by Kim et al., as the sp-d exchange interaction between the band electrons and the localized "d" electrons of the transition metal ion at the cationic site.

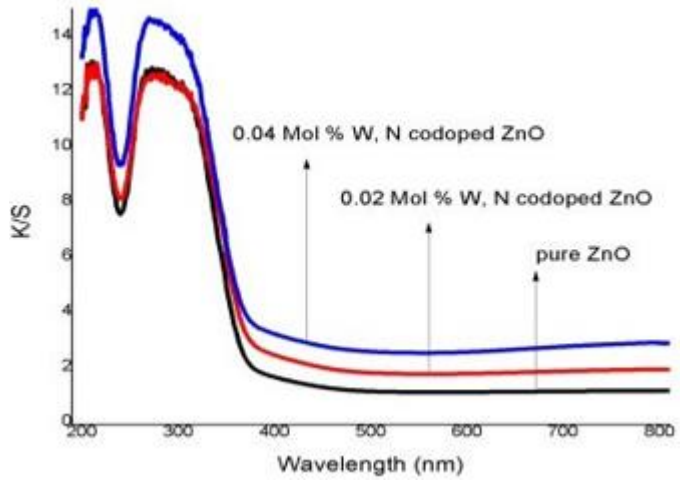


**Figure 3: Diffused Reflectance UV-Visible spectra of ZnO and W, N-codoped ZnO.**

### 3.1.4 Photoluminescence Spectra

To study the optical properties of the synthesized solar active W, N codoped ZnO, the photoluminescence (PL) spectrum is recorded at room temperature. The PL spectrum compared with pure ZnO powder and W, N codoped ZnO are shown in Figure 4.

The UV emission located at 391 nm is the band-edge emission resulting from the recombination of free excitons, and the broad green emission centered at 451 nm is caused by the radiative recombination of the photogenerated holes with electrons around the surface oxygen vacancy. In comparison with the pure spectrum of as-prepared ZnO, the UV emission of W, N codoped ZnO is enhanced, while the electron hole recombination might be suppressed. This phenomenon can be attributed to the reduction of band gap energy while doping W and N. The similar observation has been reported previously[32].

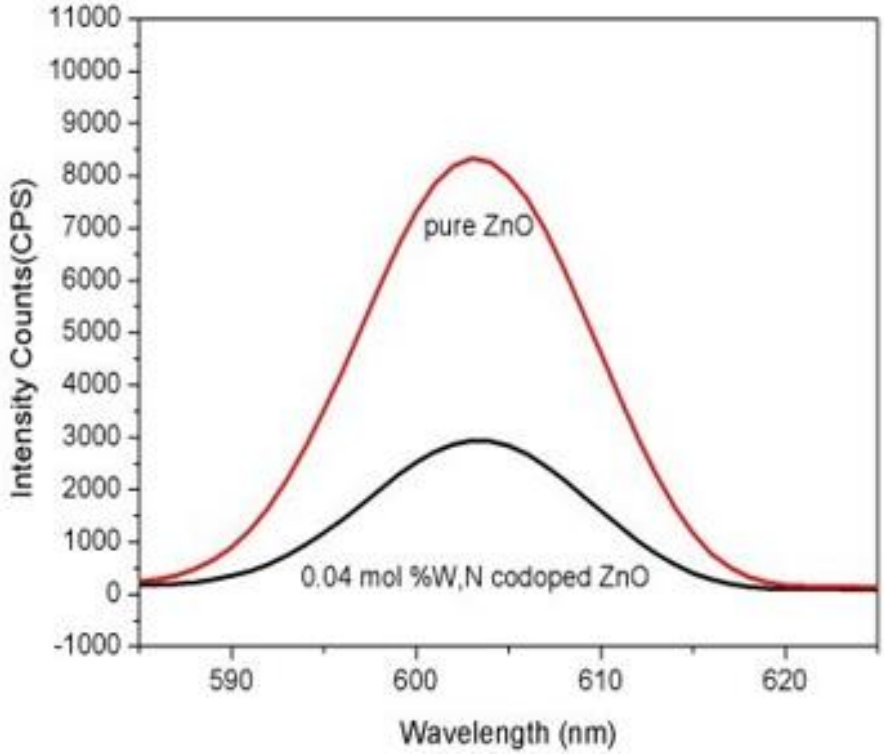


**Figure 4: Photoluminescence spectrum of pure ZnO and 0.04 mol% W, N codoped ZnO.**

### 3.1.5 FT-IR Spectroscopic Analysis

Fourier transform infrared spectroscopy of the hydrolyzed particles (Fig. 5) show strong peaks at 1564 $cm^{-1}$ and at 1399 $cm^{-1}$. The previously mentioned peak at 1564 $cm^{-1}$ indicates the formation of ZnO[33]. When tungsten doping is with ZnO, the peak value shifted to 1627, this indicates O-W bond has elongated. Peaks at 475 $cm^{-1}$ and 452 $cm^{-1}$ correspond to N-O stretching and bending. These peaks confirm integration of tungsten (W) ion and nitrogen (N) with zinc (Zn) ion.

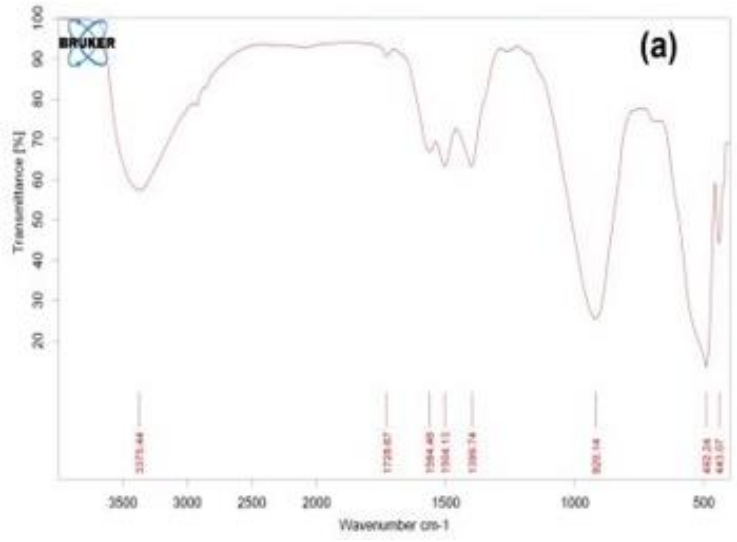

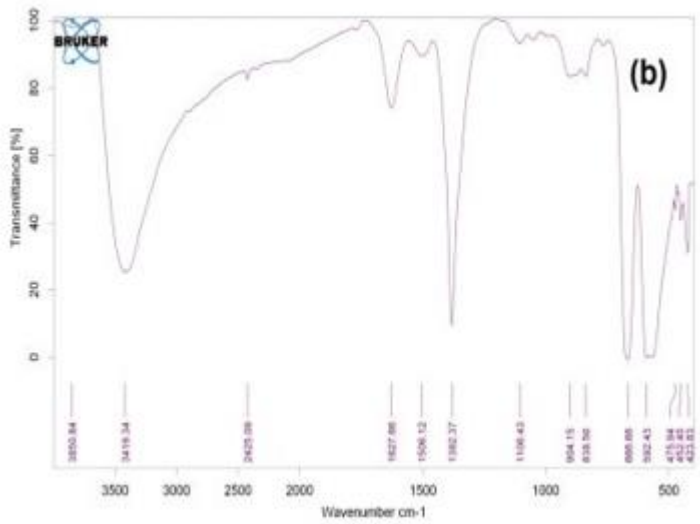


**Figure 5: FT-IR spectra of (a) pure ZnO and (b) 0.04 mol% W, N codoped ZnO photocatalyst.**

### 3.2 Photocatalytic Studies

#### 3.2.1 Photocatalytic Activity of W, N -codoped ZnO

The photocatalytic activity of the W, N-codoped ZnO photocatalysts has been evaluated from their activity in the degradation of Reactive Blue 4 (RB 4) in the presence of solar light. This dye has been chosen for the studies since it has a strong light absorption in UV-visible region. The UV-visible transmittance spectrum of the RB 4 solution show that more than 80% of incident light in the wavelength range 200-450 nm was absorbed by 50 mg·l$^{-1}$ dye solution in a path length of 1 cm. Hence, the degradation of the RB 4 solution with concentration above 50 mg·l$^{-1}$ in a simple photocatalytic process over a UV active photocatalyst like ZnO is difficult and will take more treatment time for complete degradation. The degradation of 50 mg·l$^{-1}$ RB 4 on W, N-codoped ZnO in a photocatalytic process was shown in Figure 6. The results show that W, N-codoped ZnO have higher activity than pure ZnO in simple photocatalytic process. The W, N-codoped ZnO with 0.01 mol % W, N content has shown maximum activity for the degradation of the dye and increase of W, N ion above 0.04 mol % decreases the activity of the ZnO. The high activity of the above 0.04 mol % W, N-codoped ZnO might suggest.

**$HO_2$ (hydroperoxyl radicals) are less reactive than both hydroxyl radicals and hydrogen [37].**

**Figure - 11: Effect of concentration of $H_2O_2$ on the efficiency of degradation of RB 4**

(Initial concentration $C_o$= 100 mg l$^{-1}$; pH=5; Photocatalyst dosage 1 g l$^{-1}$)

## 4. CONCLUSION

Pure ZnO and W, N codoped ZnO powder prepared in co-precipitation method followed by thermal treatment at 500°C for 5 hours has shown good activity for the degradation of reactive dyes in solar light. The prepared photocatalyst characterized by various techniques also compared them photocatalytic activity. 0.04 mol% W, N codoped ZnO demonstrated highest activity for the degradation of RB 4 with a chlorotriazine functional group. The rate of degradation of RB 4 over W, N codoped ZnO was maximum when the solution pH was 5, and the dosage of the photocatalyst was 1 g l$^{-1}$. A hydrogen peroxide concentration of 10 mM was found to be optimum for the achieving the maximum activity in a oxidant combined Photocatalytic process. The 0.04 mol% W, N codoped ZnO also has good reusability; the 0.04 mol% W, N codoped ZnO completely degraded RB 4 in 120 minutes even in oxidant combined photocatalytic processes in its fourth reuse. Hence oxidant combined photocatalytic process over 0.04 mol% W, N codoped ZnO will be an efficient and cost-effective method for the degradation of organic dyes and other organic pollutants in industrial effluent.

## 5. REFERENCES

1. M.A. Khan, A.M. Ghouri, Res. World J. Arts Sci. Commer. 2 (2011) 276.
2. B. Lellis, C.Z. Fávaro-Polonio, J.A. Pamphile, J.C. Polonio, Biotechnol. Res. Innov. 3 (2019) 275.
3. M.M. Hassan, C.M. Carr, Chemosphere 209 (2018) 201-219.

4. D. Fabbri, M.J. López-Muñoz, A. Daniele, C. Medana, P. Calza, Photochem. Photobiol. Sci. 18 (2019) 845-852.
5. D.W. Zelinski, T.P.M. dos Santos, T.A. Takashina, V. Leifeld, L. Igarashi-Mafra, Water. Air. Soil Pollut. 229 (2018) 1-12.
6. E. Regulska, D. Rivera-Nazario, J. Karpinska, M. Plonska-Brzezinska, L. Echegoyen, Molecules 24 (2019) 1118.
7. S.A. Ansari, S.G. Ansari, H. Fouad, M.H. Cho, New J. Chem. 41 (2017) 9314-9320.
8. A. Naldoni, F. Riboni, U. Guler, A. Boltasseva, V.M. Shalaev, A.V. Kildishev, Nanophotonics 5 (2016) 112.
9. U. I. Gaya, A. H. Abdullah, J. Photochem. Photobiol C., 9 (2008) 1-12.
10. J.M. Herrman, Catalysis Today, 53 (1999) 115-129.
11. C. Shifu, Z. Wei, Z. Sujuan, L. Wei, Chem. Eng. J., 148 (2009) 263-269.
12. D. Chatterjee, D. Shimanti, Photochem. Rev., 6 (2005) 186-205.
13. S. Saktihvel, M. Janczarek, H. Kisch, J. Phys. Chem., 108 (2004) 19384-19387.
14. M. Pera-Titus, V. Gar'cia-Molina, M. Baños, J. Gim'enez, S. Esplugas, Appl. Catal B:Environ., 47 (2004) 219-256.
15. U. Poornaprakash, K. Chalapathi, S.V. Subramanyam, Y. Prabhakar Vattikuti, S.P. Shun, Mater. Res. Express 6 (2019) 105356.
16. B. Poornaprakash, U. Chalapathi, P.T. Poojitha, S.V.P. Vattikuti, M.S.P. Reddy, J. Mater. Sci. Mater. Electron. 30 (2019) 9897-9902.
17. M. Kaur, A. Umar, S.K. Mehta, S. Singh, S.K. Kansal, H. Fouad, O.Y. Alothman, Material 11 (2018) 2254.
18. C. Díaz-Uribe, J. Viloria, L. Cervantes, W. Vallejo, H. Navarro, E. Romero, C. Quiñones, Int. J. Photoenergy 2018 (2018) 1-8.
19. B. Poornaprakash, U. Chalapathi, P.T. Poojitha, S.V.P. Vattikuti, S.H. Park, J. Supercond. Nov. Magn. 33 (2020) 539-544.
20. C. Diaz-Uribe, W. Vallejo, G. Camargo, A. Muñoz-Acevedo, C. Quiñones, E. Schott, E. X. Zarate, J. Photoc. Photobiol. A Chem. 2019, 384, 112050.
21. D.G. Fan, R. Zhang, Y. Li, Solid State Commun. 39 (2010) 1911-1914.